Chapter 3

Enhanced photo conversion efficiency of a hybrid bulk heterojunction device based on poly(3-octylthiophene)/zinc oxide nanocomposite

GRAPHICAL ABSTRACT

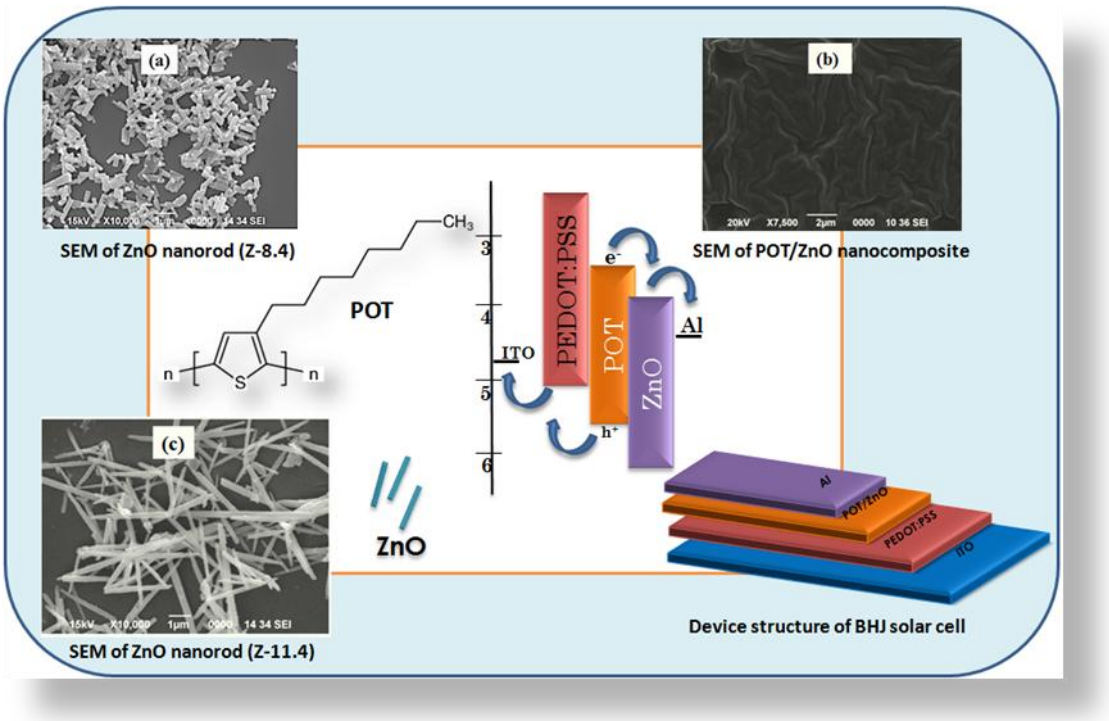

The high aspect ratio ZnO nanorods exhibit significant photovoltaic performance in POT/ZnO based BHJ devices

3.1 Introduction

Throughout the years conjugated polymer nanocomposite material based hybrid bulk heterojunction (BHJ) devices received the increasing demand for a low cost device because of their easy processability, light weight and flexibility. Among various conjugated polymers, poly (3-octylthiophene) (POT) has been widely used as the polymer is easily processable and their favourable optoelectronic properties.[1-3] In general, nanocomposite material combines the superior properties of both the components such as easy processability, light weight and flexibility, high electron mobility, size dependent optical properties, physical and chemical stability of the nanofiller etc.[4] Due to the synergistic effect between POT and the inorganic nanofiller, their nanocomposite provides an improved performance than their individual components. Photovoltaic devices based on zinc oxide (ZnO) nanocrystals[5-12] offer superior performance due to their ease of preparation, wide band gap, size dependent optoelectronic properties, thermal and chemical stability and eco-friendliness. Recently, many researchers are focusing on photovoltaic devices based on hybrid of poly (3-alkylthiophene) and other materials.[2, 3, 13-20] However, a very few studies have been carried out regarding the photovoltaic performance of POT/ZnO nanocomposites.

Taking into account of these aspects, an effort was made in combining POT and ZnO nanorods to form a new nanocomposites material through chemical reaction. The nanocomposites formation is confirmed by Fourier transform infra-red spectroscopy (FT-IR) and scanning electron microscopy-energy dispersive X-ray spectroscopy (SEM-EDX). Ultraviolet-visible (UV-visible) analysis shows a good light harvesting ability of the nanocomposites material in the visible range. The oxidation/reduction potential becomes lower than their individual components, which is confirmed by cyclic voltammetry (CV) analysis. Aspect ratio of ZnO nanorods has a pronounced effect on the photovoltaic property of the system. Photovoltaic measurement of the fabricated device shows that maximum photo conversion efficiency (PCE) of 1.33% can be attained in the device for maximum aspect ratio 20 of ZnO nanorods.

3.2 Experimental

3.2.1 Reagents

The chemicals Zinc acetate [$Zn(CH_3COO)_2$], sodium hydroxide (NaOH), cetyl trimethyl ammonium bromide (CTAB), chloroform, chlorobenzene and methanol were purchased from Merck. 3-octylthiophene (3OT), ferric chloride ($FeCl_3$), Poly (3,4-ethylenedioxythiopene): poly (styrenesulfonate) (PEDOT:PSS), [6,6]-Phenyl-C_{61}-butyric acid methyl ester (PCBM) and indium tin oxide (ITO) coated glasses were purchased from Sigma Aldrich.

3.2.2 Synthesis of ZnO nanorods

Three sets of ZnO nanorods were synthesized by a one pot hydrothermal method.[5] First, a solution was prepared by adding $Zn(CH_3COO)_2$ and CTAB in distilled water at a fixed molar ratio of 1:1.5. To this solution, 0.6 M NaOH (aq) solution was added dropwise, by maintaining the pH of the solution in the range 8.4-11.4. Then the mixture was transferred to a Teflon-lined autoclave and kept into a hot air oven at 100 °C. After a defined time period (16 h), the autoclave was allowed to cool. Products were filtered with distilled water and ethanol to remove the un-reacted surfactant and dried under vacuum at 50 °C. The synthesized ZnO nanorods were denoted as Z-8.4, Z-10.4 and Z-11.4 respectively, where the numeral determines the pH of the medium.

3.2.3 Synthesis of Poly(3-octylthiophene) (POT)

The polymer POT was synthesized by an oxidative polymerization method mentioned in the literature.[3] In a 100 mL round-bottomed flask 0.03 mol $FeCl_3$ was added into 20 mL chloroform under nitrogen and allowed to stir for ~15 min. The monomer 3OT was gradually added dropwise to the solution and the reaction was continued at 25 °C for 7 h. After the reaction, the product was precipitated in methanol, filtered and dried. The product was dissolved in chloroform (50 mL). By removing the solvent through rotary evaporation, a greenish black film was obtained. The film was added to methanol in order to remove the unwanted residue, and then dried under vacuum. Finally, by Soxhlet extraction with methanol for 20 h, followed by drying in vacuum the pure polymer film was obtained.

3.2.4 Synthesis of POT/ZnO nanocomposites

0.1 g pre-synthesized POT was added into a round-bottomed flask under vacuum for

30 min. 4 mL chloroform was gradually added into the flask and solution was ultrasonicated for 30 min in vacuum. A dispersion of 20 wt% pre-synthesized ZnO nanorod in 10 mL methanol was added dropwise into the solution and stirred for 30 min. The product was vacuum dried and collected for further characterization and application. A set of nanocomposites was prepared following the same procedure using the ZnO nanorods at different pH (Z-8.4, Z-10.4 and Z-11.4). For convenience, all the nanocomposites are denoted by ZPOT-8.4, ZPOT-10.4 and ZPOT-11.4 respectively, where the number in bracket denotes the respective pH.

3.2.5 Fabrication of the photovoltaic device

A set of bulk heterojunction photovoltaic devices was fabricated in a typical sandwich structure of ITO/PEDOT:PSS/(POT/ZnO nanocomposite)/Al. The summary of the fabrication process is as follows: the ITO-coated glass substrates (resistivity: 15-20 Ω-cm) were cleaned by ultrasonic treatment in detergent, de-ionized water and acetone respectively and dried. The ITO layer from the substrates was etched completely from one end (~ 5 mm) by the acid treatment. The cleaning of the substrates was repeated. Then a thin layer of PEDOT:PSS (thickness 10 nm) was spin coated onto the ITO coated glass followed by thermal treatment at 120 $^{\circ}$C for 30 min. A solution containing the nanocomposite in 1 mgmL^{-1} ratio in chloroform was prepared under ultrasonication and spin coated at a rotation speed of 1800-2000 rpm, onto the surface of PEDOT:PSS with a thickness of 50-80 nm. To improve the film quality, the nanocomposite film was thermally treated at 120 $^{\circ}$C for 30 min at a vacuum oven. Finally, aluminium cathode was thermally evaporated in a vacuum coating unit at a pressure of 4x10^{-5} Pa. The active area of the device was 1cm^2. Likewise, a set of devices has been fabricated by using all the nanocomposites (ZPOT-8.4, ZPOT-10.4 and ZPOT-11.4). For comparison, a device with the pristine polymer was fabricated using PCBM in 1:1 weight ratio with POT.

3.3 Instruments and methods

3.3.1 Scanning electron microscopy (SEM)

Surface morphology of the synthesized nanorods and nanocomposite was carried out

by JSM-6390LV (JEOL, Japan) scanning electron microscope (SEM) at an accelerating voltage of 5-15 kV. The surface of the sample was Pt coated before observation in SEM.

3.3.2 Fourier transform infrared spectrometer (FT-IR)

Fourier transform infrared spectra (FT-IR) of the polymer nanocomposites were collected by FT-IR Nicolet, (Impact 410) spectrophotometer (USA). Pellets were prepared by a compression moulding under vacuum where a required amount of samples was grounded and mixed properly with dried KBr to form the pellet. The spectra were recorded in transmission mode in the range of 4000-400 cm^{-1} with a nominal resolution of 4 cm^{-1}.

3.3.3 Ultraviolet-visible spectroscopy (UV-visible)

Optical absorption spectra of the products were recorded in a Shimadzu UV-2550 ultraviolet-visible spectrophotometer, taking chloroform as solvent and a wavelength scan in the range of 200-800 nm.

3.3.4 Thermogravimetric analysis (TGA)

Thermal properties of the polymer and nanocomposites were revealed by a Shimazdu TGA 50 thermal analyzer at a heating rate of 10 °C min^{-1}. Analysis was carried out at a temperature ranging from 25 °C to 600 °C under inert atmosphere of nitrogen with flow rate of 30 mL min^{-1}.

3.3.5 Cyclic voltammetry (CV)

Cyclic voltammetry (CV) study was carried out in an electrochemical work-station (Model: Sycopel AEW2_10) equipped with three electrodes Ag/AgCl electrode (reference), platinum wire (counter) and glassy carbon electrode (working). Electrochemical characteristics of the polymer and nanocomposites were investigated by CV scanning in 0.1 M lithium perchlorate ($LiClO_4$) supporting electrolyte solution in acetonitrile at a scan rate of 20 mVs^{-1}. The HOMO and LUMO energy levels as well as the energy gap (E_g^{ec}) can be calculated from the onset oxidation potentials (ϕ_{ox}) and the onset reduction potentials (ϕ_{red}) according to the following equations [Eqn. 3.1-3.3]

$$\text{HOMO} = -(\phi_{ox} + 4.71)\ \text{eV} \qquad \text{Eqn. 3.1}$$

$$\text{LUMO} = -(\phi_{red} + 4.71)\ \text{eV} \qquad \text{Eqn. 3.2}$$

$$E_g^{ec} = (\phi_{ox} - \phi_{red})\ \text{eV} \qquad \text{Eqn. 3.3}$$

3.3.6 Photovoltaic study

Photovoltaic characterization of fabricated solar cells was carried out under simulated (AM1.5) solar illumination at 1 sun (100 mW/cm^2) in laboratory air. The device parameters are calculated using the following equations [Eqn. 3.4-3.6]

$$\text{Fill factor, FF} = \frac{J_{max}.V_{max}}{J_{sc}.V_{oc}} \qquad \text{Eqn. 3.4}$$

$$\text{Maximum power, } P_{max} = J_{max}.V_{max} = J_{sc}.V_{oc}.FF \qquad \text{Eqn. 3.5}$$

$$\eta = \frac{P_{max}}{P_{in}} = \frac{J_{sc}.V_{oc}.FF}{P_{in}} \qquad \text{Eqn. 3.6}$$

where, J_{max} and V_{max} are the current density and voltage respectively at the maximum power point of the J-V curve. J_{sc} and V_{oc} are the short circuit current density and open circuit voltage respectively. FF is the fill factor. P_{in} is the intensity of the white light and η is the photo conversion efficiency (PCE) of the device.

3.4 Results and discussion

3.4.1 Size and morphology (SEM-EDX)

Fig. 3.1 shows the rod-shaped morphology of the synthesized ZnO nanorods with an average diameter of 155-188 nm. In the hydrothermal synthesis of ZnO nanorods, the pH of the reaction medium plays an important role. When we increase the pH to 10.4, both the concentrations of Zn^{2+} and OH^- become considerable. Therefore, particle growth takes place both in longitudinal and transverse direction, as a consequence of which both the diameter and length of the nanorod increase with increase in pH. At the pH above 10.4, the excess OH^- concentration dominates Zn^{2+} concentration and therefore particle growth occurs significantly in the longitudinal direction.[3]

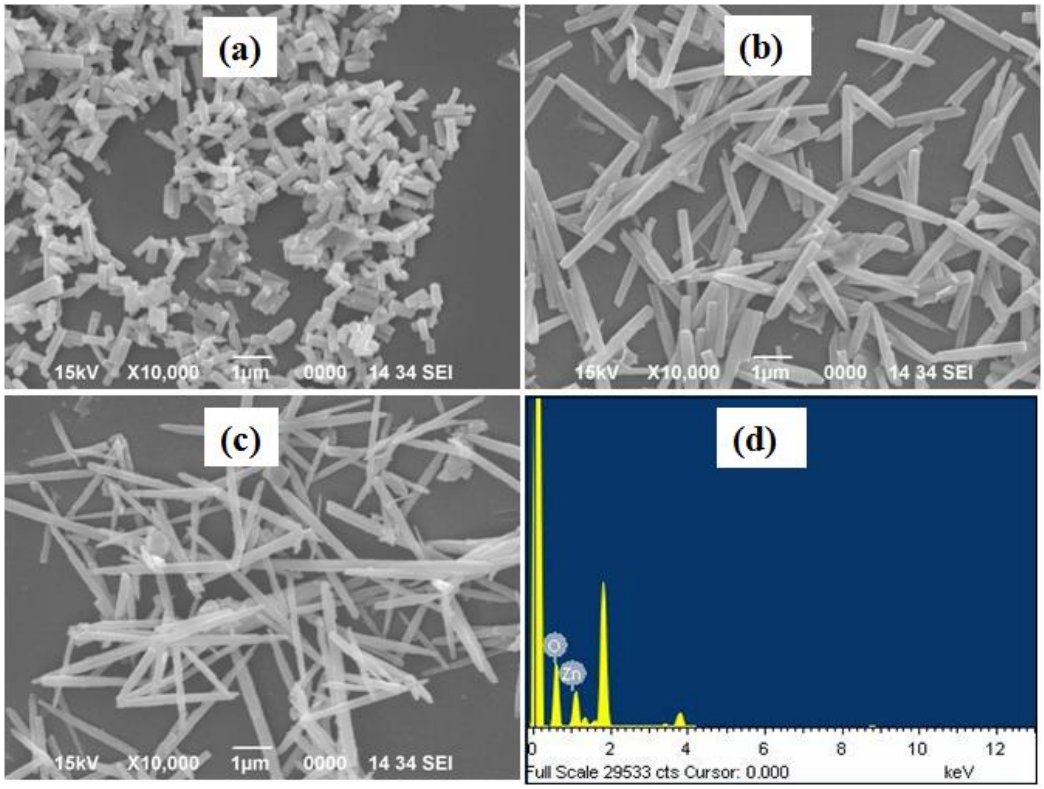

Fig. 3.1 SEM images of (a) Z-8.4, (b) Z-10.4, (c) Z-11.4, (d) EDX spectrum of Z-11.4. *The number denotes the respective pH of the medium

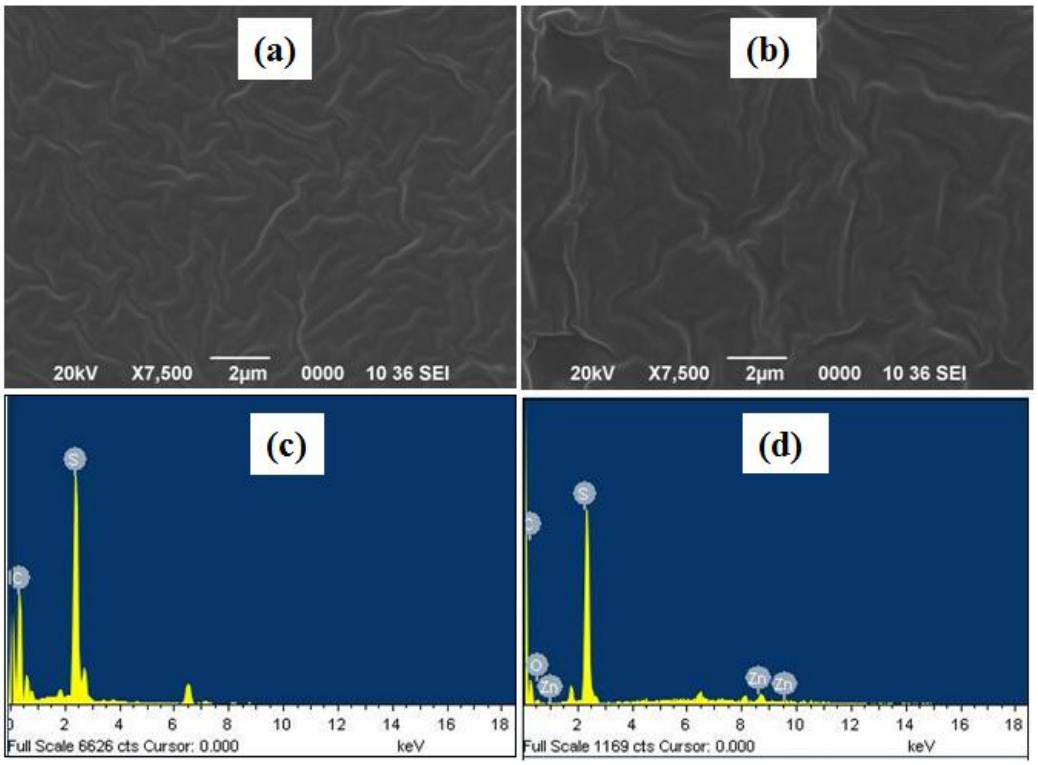

Fig. 3.2 SEM images of (a) POT, (b) ZPOT-11.4; EDX spectra of (c) POT, and (d) ZPOT-11.4. *The number denotes the respective pH of the medium

It causes significant increase in aspect ratio of the nanorods. For instance, it is observed that aspect ratio of Z-8.4 nanorod is 8, while it is 20 for Z-11.4. EDX spectrum of ZnO nanorods (Z-11.4) shows the presence of both Zn and O atoms in the nanostructure that confirms the successful formation of ZnO nanorods [Fig. 3.1d].

The formation of the nanocomposite as well as its morphology is determined by SEM-EDX analysis [Fig. 3.2]. It is observed that the surface of POT becomes more homogeneous and smooth after the incorporation of the nanofiller into the polymer. Moreover, ZnO nanorods are properly mixed with the polymer matrix. Successful formation of the nanocomposites was determined by EDX study [Fig. 3.2c, d].

3.4.2. Structural (FT-IR) analysis

Structural characteristic of POT with or without ZnO nanorod is investigated by FT-IR analysis [Fig. 3.3] and summary of the results are shown in Table 3.1. In the spectra of POT, all the characteristic peaks are found at around 3447 cm^{-1}, 2923 cm^{-1} and 2852 cm^{-1}, 1631 cm^{-1} and 1458 cm^{-1}, 1350 cm^{-1}, 1019 cm^{-1} and 829 cm^{-1} which are due to O-H stretching, Symmetric and asymmetric (-CH_2 or –CH_3), C=C stretching of thiophene ring, C-H stretching partial C=S stretching, C-H_β out-of-plane bending of 2,3,5-trisubstituted thienylene moiety respectively.[21] This confirms the successful polymerization of 3-octylthiophene. All the characteristic peaks are found in the nanocomposites with a slight shift towards higher wavenumber. A modification in the electronic structure of the polymer arises in presence of the ZnO nanorods due to which peaks shift towards higher wavenumber. Moreover, in the finger print region an additional absorption band is observed at around 505-749 cm^{-1} in all the nanocomposites which can be assigned to the Zn-O stretching arising in presence of the nanostructure.[5]

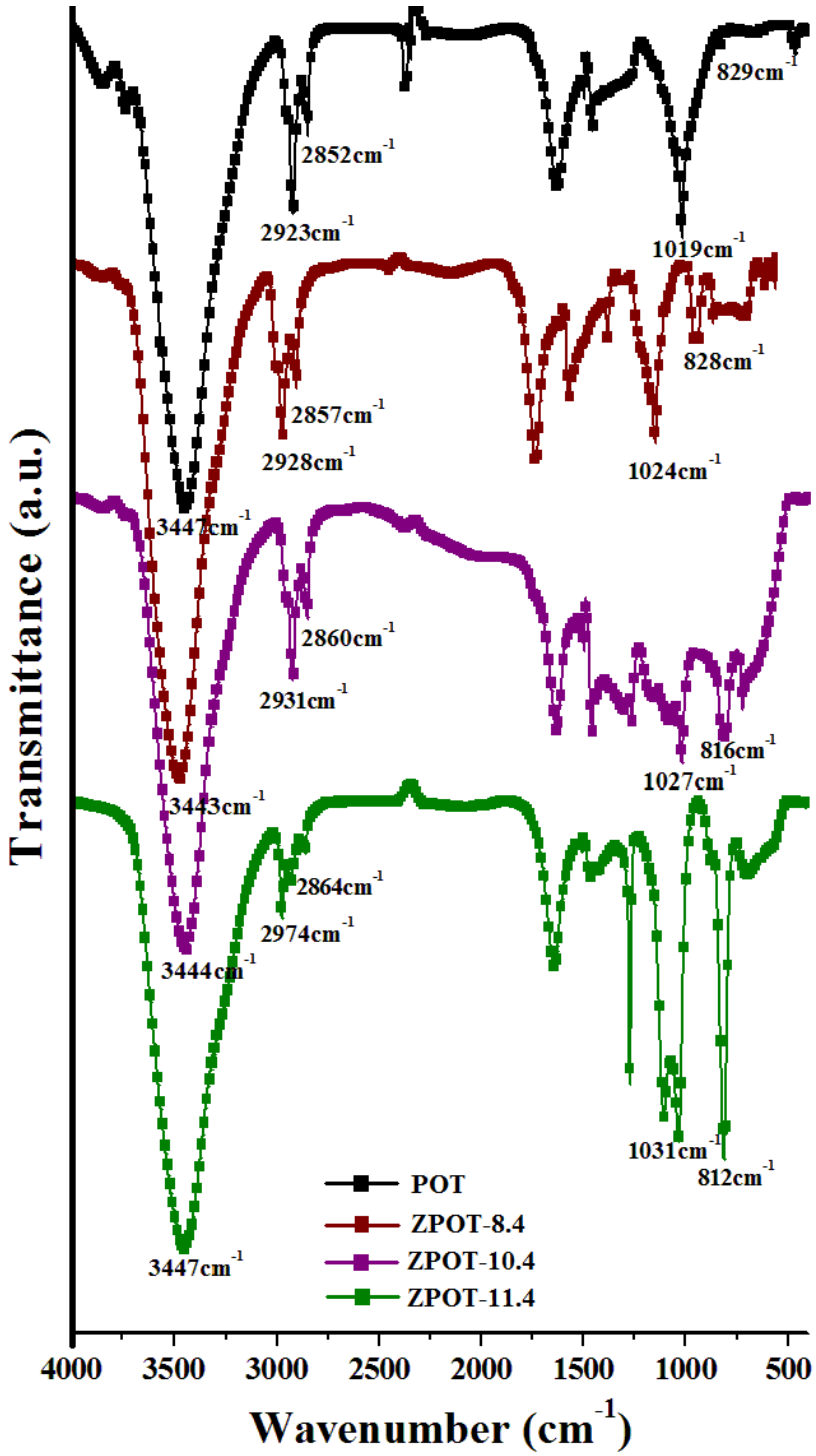

Fig. 3.3 FT-IR spectra of polymer and nanocomposites with different aspect ratio ZnO nanorods. *The number denotes the respective pH of the medium

Table 3.1 Characteristic vibrational modes for the nanocomposites

Characteristic bond	Wavenumber (cm^{-1})			
	POT	ZPOT-8.4	ZPOT-10.4	ZPOT-11.4
-OH stretching	3447	3443	3444	3447
Symmetric C-H stretching (-CH_2 or –CH_3)	2923	2928	2931	2974
Asymmetric C-H stretching (-CH_2 or –CH_3)	2852	2857	2860	2864
Thiophene ring C=C stretching	1631 and 1458	1636 and 1459	1640 and 1465	1642 and 1467
C=S (partial) stretching	1350	1267	1270	1272
C-H_β out-of-plane bending of 2,3,5-trisubstituted thienylene moiety	1019 and 829	1024 and 828	1027 and 816	1031 and 812
Z-O stretching	---	507-749	505-752	506-747

3.4.3 Optical study (UV-visible spectroscopy)

The UV-visible spectra for POT and POT/ZnO nanocomposites synthesized with a set of ZnO nanorods prepared at different pH (Z-8.4, Z-10.4 and Z-11.4) are shown in Fig. 3.4 (a). It is observed that POT shows an absorption maximum at ~423 nm due to $\pi \rightarrow \pi^*$ transition.[3] A remarkable change is observed in the optical spectra of the nanocomposites [Fig. 3.4 (a)]. The peak due to $\pi \rightarrow \pi^*$ transition is also observed in the nanocomposites with a slight shift in the absorption maxima towards higher wavelength. It strongly provides an evidence for the modification of the electronic structure of POT in presence of ZnO nanorods. This reduces the optical band gap of the polymer [Table 3.2]. ZnO nanorods can form localized electronic states between HOMO and LUMO levels of the polymer thus altering the electronic states of the polymer. This leads to the observed change in the optical band gap.[22] With increase in aspect ratio of the nanorods, more number of localized electronic states is formed thus leading to further decrease in optical band gap [Fig. 3.4 (b)].

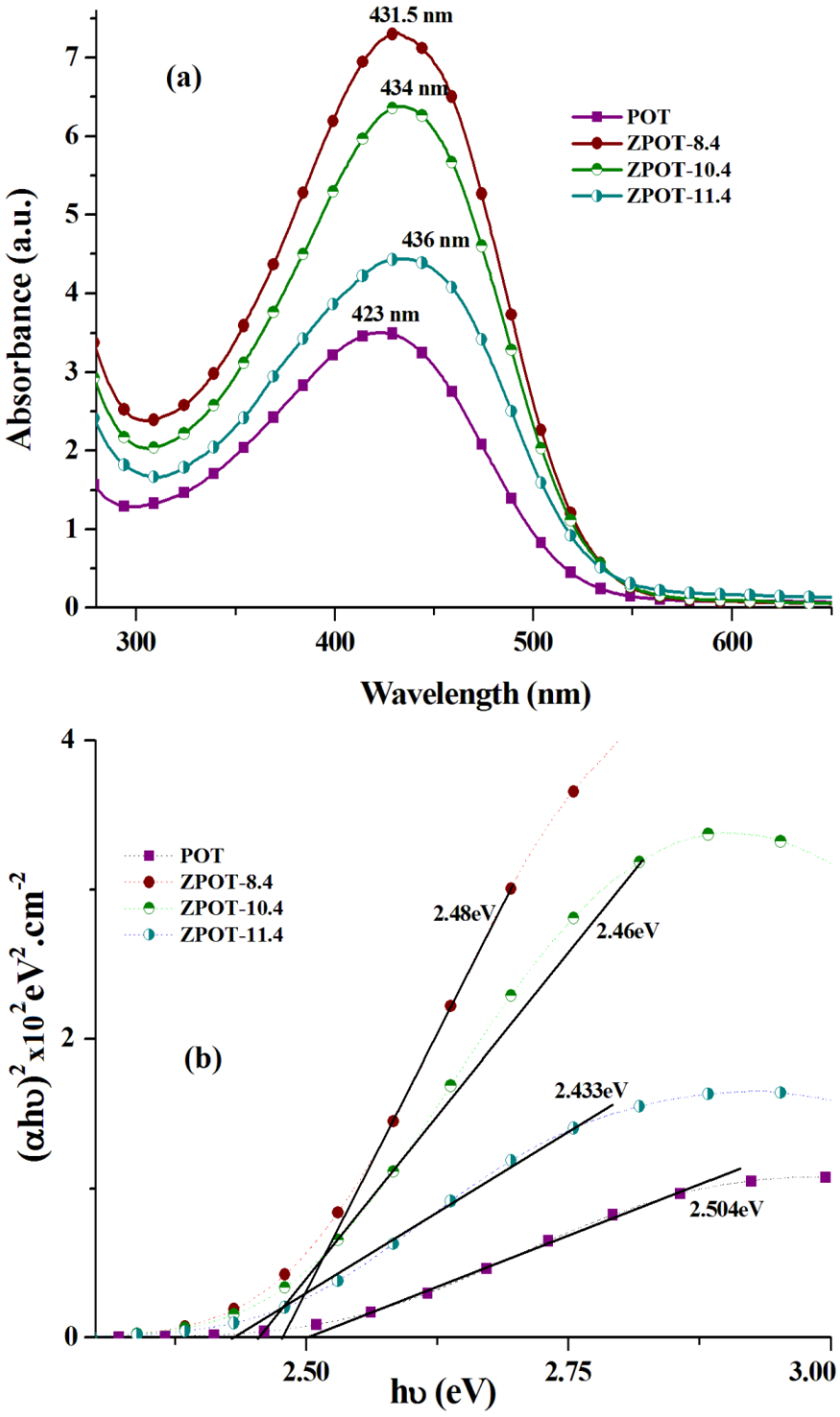

Fig. 3.4 (a) UV-visible spectra and (b) respective band gap diagram of polymer and nanocomposites with different aspect ratio ZnO nanorods.

*The number denotes the pH of the medium

Table 3.2 Optical and electrochemical properties of the polymer and the nanocomposites

Sample particulate	E_g^{op} (eV)	E_g^{ec} (eV)	HOMO (eV)	LUMO (eV)
POT	2.50	1.64	-5.51	-3.87
ZPOT-8.4	2.48	1.59	-5.55	-3.96
ZPOT-10.4	2.46	1.25	-5.51	-4.26
ZPOT-11.4	2.43	1.23	-5.57	-4.34

3.4.4 Thermogravimetric analysis (TGA)

Thermogravimetric analysis (TGA) is proven to be the most effective tool to study the thermal stability of a polymer which can determine whether the material is suitable for device fabrication. The thermal stability of the synthesized nanocomposites are investigated by using TGA and the weight loss traces recorded in the temperature range 25-600°C as shown in Fig. 3.5. The thermal stability values are summarized in Table 3.3. An enhanced thermal stability can be seen for all the nanocomposites. For instance, in the pristine polymer shows the major degradation occurs at 471 °C, while for the nanocomposites it is in the range of 476-484 °C [Table 3.3].

The reason of the thermal degradation of a polymer can be ascribed to the formation of free-radicals at the weak chains followed by the radical transfer from chain-to-chain via inter-chain reactions. The enhancement in the thermal stability occurs in the nanocomposites due the reduced mobility of the polymer chain in presence of the nanofiller. The reduced chain mobility causes delay in the degradation process.[5, 23]

The strong interaction between ZnO nanorods and POT is said to be solely responsible for this behaviour. Moreover, the nanofiller within the polymer matrix may impede the mass transport of the volatile products generated during degradation process which offers high thermal stability to the nanocomposite.[24] From Table 3.3 it is observed that with increase in the aspect ratio of the nanorods, the thermal stability of the nanocomposite increases. The better thermal stability of the high aspect ratio nanorods may be illustrated by the formation of more effective mass transport barrier to the volatile products.[25, 26.]Similar results were obtained elsewhere.[24, 27] The

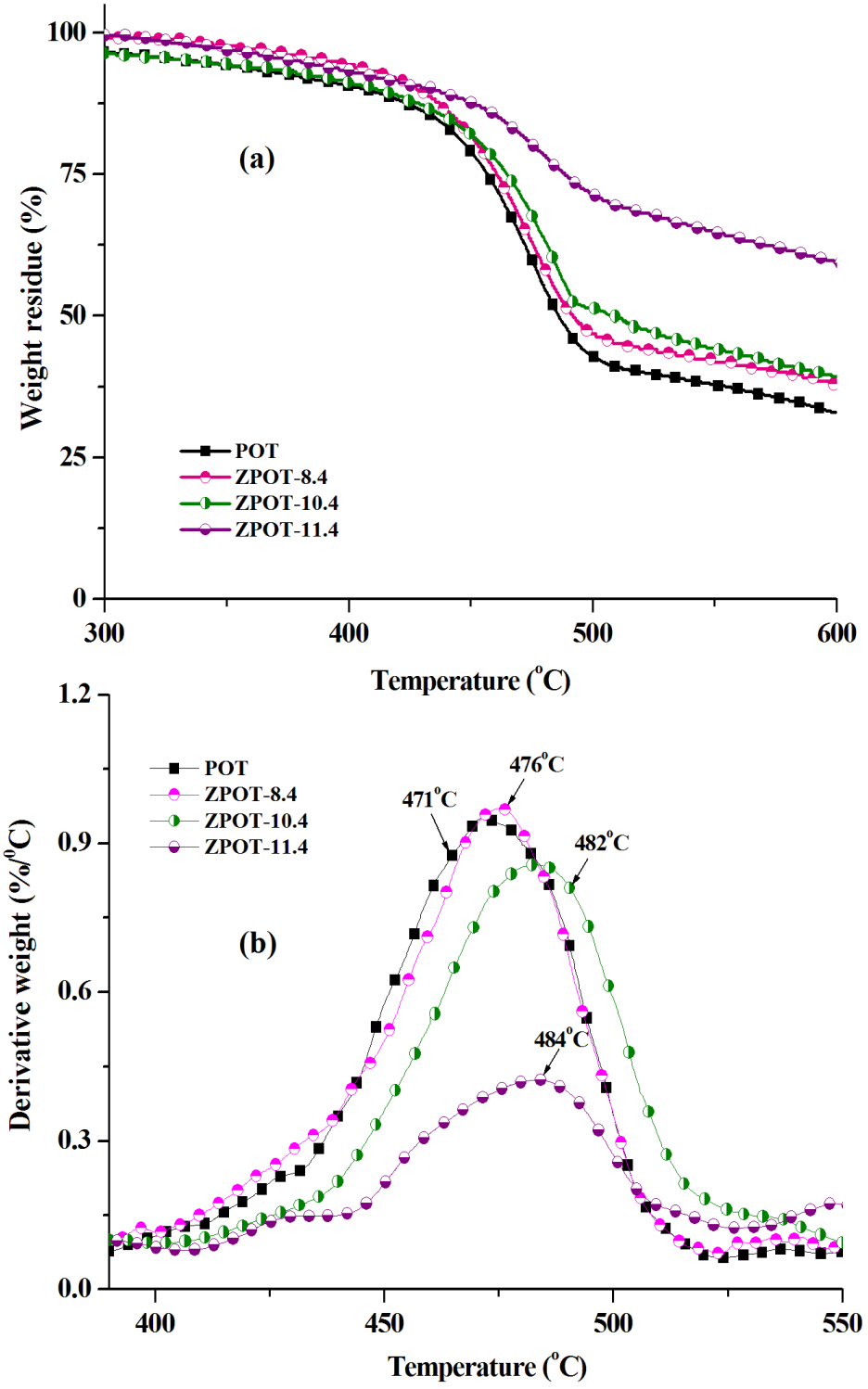

Fig. 3.5 (a) TGA and (b) DTG curves of polymer and nanocomposites with different aspect ratio ZnO nanorods.* The number denotes the pH of the medium

nanocomposites also show higher char content at 600 °C than their pristine polymer [Table 3.3]. Thus, we can say that the incorporation of the ZnO nanorods results in

significantly improved thermal stability of the nanocomposites.

Table 3.3 The TGA values of the polymer and the nanocomposites

Sample code	Major degradation temperature T_d (°C)	Char content (%)
POT	471	33
ZPOT-8.4	476	38
ZPOT-10.4	482	40
ZPOT-11.4	484	59

3.4.5 Electrochemical analysis (CV)

To study the redox behavior of the the nanocomposites as well as to estimate their electrochemical band gap, cyclic voltammetry (CV) analysis was performed [Fig. 3.6]. CV peaks at positive potential are assigned to oxidation, whereas peaks at negative potential correspond to reduction. The HOMO and LUMO energy levels as well as the

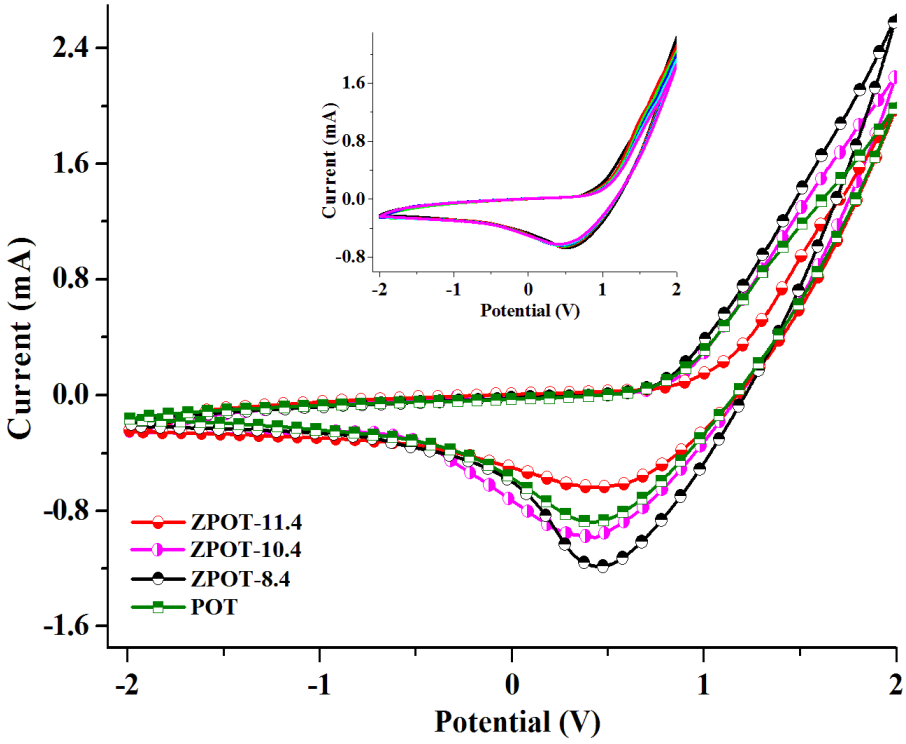

Fig. 3.6 Cyclic voltammetry curves of polymer and nanocomposites with different aspect ratio ZnO nanorods. Inset shows CV curves of ZPOT-11 showing 50 repeated cycles.*The number denotes the pH of the medium

energy gap (E_g^{ec}) can be calculated from the onset oxidation potentials (φ_{ox}) and the onset reduction potentials (φ_{red}) according to the equations [Eqn. 3.1-3.3].

From Fig. 3.6, it is observed that the electrochemical band gap of the polymer is significantly reduced by a maximum value of 0.41 eV in presence of the nanofiller [Table 3.2]. From the table, it may be illustrated that the interaction of ZnO nanorods with the polymer matrix modifies the electronic structure of the polymer. ZnO nanorods can form localized electronic states between HOMO and LUMO levels of the polymer thus lowering the energy of the LUMO level significantly as the HOMO level energy remains almost same. This reduces the electrochemical band gap of the polymer [Table 3.2].[22] With increase in aspect ratio of the nanorods, more number of localized electronic states are formed thus leading to further decrease in band gap [Fig. 3.6]. Same trend appears in case of the optical band gap of the polymer [Table 3.2]. A remarkable electrochemical reversibility is observed in the nanocomposite even after 50 repeated cycles [Fig. 3.6 inset]. This reveals that the cathodic and the anodic peaks are nearly symmetrical above each other in the nanocomposite with minimum separation. Further we can say that the charge capacity remains almost unchanged after few repeated cycles and it does not get diminished even after number repeated cycles. This property emphasizes that POT/ZnO nanocomposite can be efficiently used to fabricate a BHJ photovoltaic device.

3.4.6 Study of photovoltaic performance

In order to study the effect of aspect ratio of ZnO nanorods on device performance, J-V characteristics of the BHJ devices have been performed [Fig. 3.7 (a)]. The devices are tested under simulated AM 1.5 illumination at 100 mW/cm^2 intensity. From the J-V characteristics of the devices all the device parameters can be estimated using the equations [Eqn. 3.4-3.6]. The results are summarized in Table 3.4.

The POT/ZnO nanocomposite shows better PCE in the range 0.75-1.33%, which is only 0.22% for pristine POT. This can be explained in terms of energy levels. In a polymer nanocomposite based BHJ device, the polymer plays the role of the donor and the semiconductor nanofiller acts as the electron acceptor. When the polymer absorbs sunlight, excitons are generated in the active layer. An exciton is defined as the

electron-hole pair bound by strong coulombic interaction and it has a very little mobility that can easily recombine. Hence, for efficient charge separation by the respective electrodes in the device, the active layer should contain an acceptor material.

The morphology of ZnO nanorods has a significant influence on device performance. The hopping events occurred during the electron transport towards the cathode are

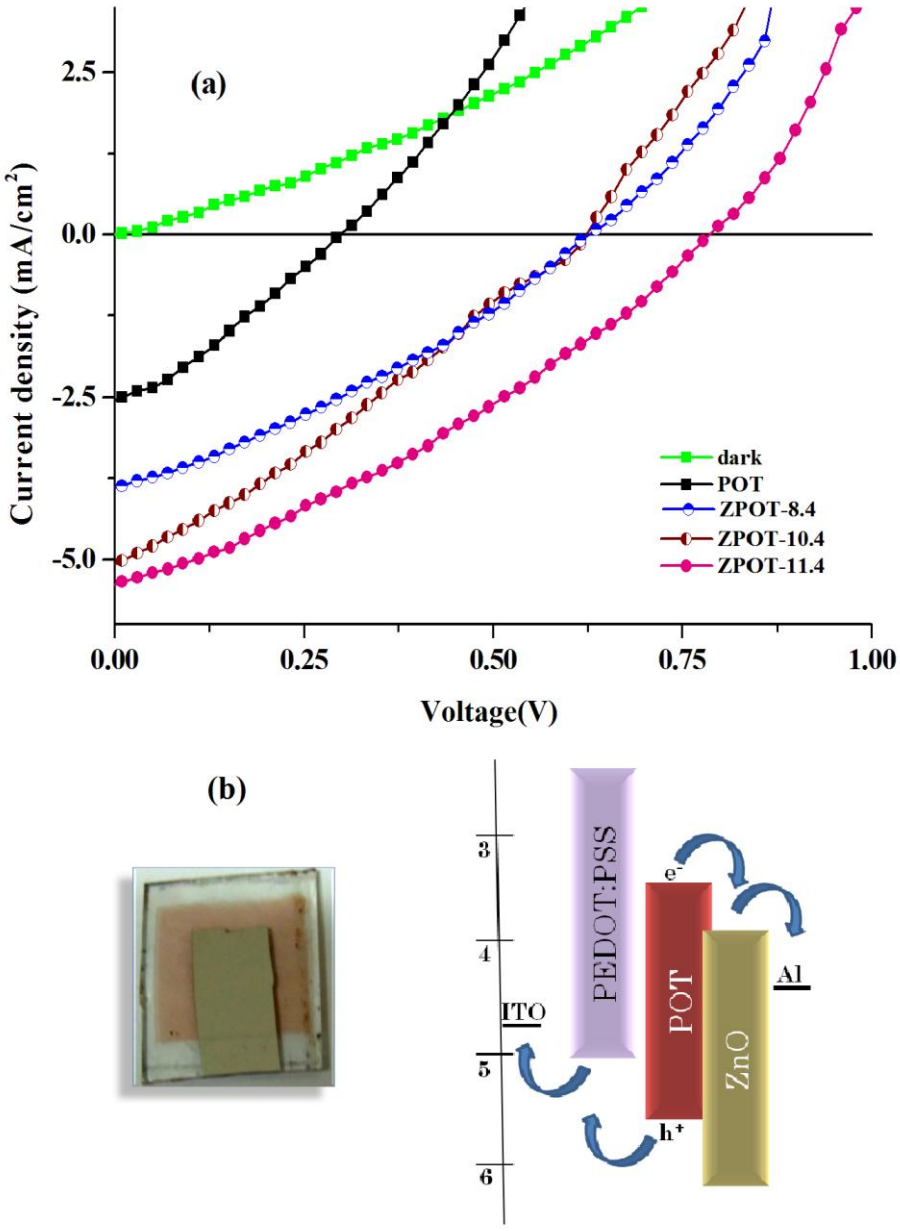

Fig. 3.7 (a) J-V curves of the fabricated devices under illumination (*the number denotes the pH of the medium), (b) photograph and energy level diagram of the device

Table 3.4 Photovoltaic characteristics of devices with different aspect ratio ZnO nanorods

Device	V_{oc} (V)	J_{sc} ($mAcm^{-2}$)	FF	PCE %
POT:PCBM	0.30	2.55	0.29	0.22
ZPOT-8.4	0.63	3.90	0.31	0.75
ZPOT-10.4	0.63	5.09	0.28	0.88
ZPOT-11.4	0.79	5.37	0.32	1.33

restricted in presence of the nanorods. This reduces the possibility of charge recombination, thus offering high PCE.[15]

Table 3.4 shows the variation of different photovoltaic parameters with aspect ratio of ZnO nanorods. It is observed that with increase in aspect ratio, there is an apparent increase in J_{sc} in the device. This variation can be illustrated by the increased charge formation in the nanocomposite with increase in aspect ratio.[9] Additionally, more percolation pathways may form in the longer nanorods which improve the transport of electrons. Thus, it can provide better photocurrent in the device.[9] In all the nanocomposite devices the FF and V_{oc} have almost constant values. Therefore, the increased value of J_{sc} has a great influence on increasing the PCE of the devices.[28]

For comparison, we have fabricated a device with the pristine polymer where PCBM in 1:1 weight ratio was taken as the electron acceptor. It is observed that ZnO has the better electron accepting ability than PCBM. As we can see from Fig. 3.7 (b), the LUMO levels of the polymer and ZnO are closer, dissociated electrons can efficiently be transported to the respective electrodes. Therefore, the devices show higher PCE (0.75-1.33%) than their pristine counterpart (0.22%).

3.5 Conclusion

- POT/ZnO nanocomposites have been synthesized by a chemical method.
- A set of BHJ device has been fabricated by using the POT/ZnO nanocomposite as the active layer.
- The incorporation of high aspect ratio ZnO nanorods results in increased charge formation in the nanocomposite that offer high value of J_{sc}.

- More percolation pathways may form in the longer nanorods which improve the transport of electrons. Thus, it can provide better photocurrent in the device.
- The overall study suggests that ZnO nanorod of aspect ratio 20 is the best candidate for obtaining a PCE of 1.33% in a set of BHJ device.

References

1. Dierckx, W., et al. *J. Mater. Chem. C* **2**, 5730-5746, 2014.
2. Arenas, M.C., et al. *Sol. Energy Mater. Sol. Cells* **94**, 29-33, 2010.
3. Han, Z., et al. *Sol. Energy Mater. Sol. Cells* **95**, 483-490, 2011.
4. Nguyen, B.P., et al. *J. Nanomater.* **26**, 1-20, 2014.
5. Sharma, S., et al. *J. Polym. Mater.* **32** (2), 179-197, 2015.
6. Ravirajan, P., et al. *J. Phys. Chem. B* **110**, 7635-7639, 2006.
7. Shoaee, S., et al. *Adv. Mater.* **26**, 263-268, 2014.
8. Ghosh, M., et al. *arXiv preprint arXiv:1008.0112*, 2010.
9. Suresh, P., et al. *Sol. Energy Mater. .Sol. Cells* **92**, 900-908, 2008.
10. Liu, J.P., et al. *Chem. Phys. Lett.* **470**, 103-106, 2009.
11. Sharma, G.D., et al. *Sol. Energy Mater. Sol. Cells* **90**, 933-943, 2006.
12. Briscoe, J., et al. *J. Phys.: Conf. Ser.* **476**, 012009(1-5), 2013.
13. Gu, Z., et al. *polymers* **3**, 558-570, 2011.
14. Miyanishi, S., et al. *Macromolecules* **45**, 6424-6437, 2012.
15. Bouclé, J., et al. *C. R. Physique* **9**, 110-118, 2008.
16. Wang, M., & Wang, X. *Sol. Energy Mater. Sol. Cells* **92**, 766-771, 2008.
17. Hu, H., et al. *Sol. Energy Mater. Sol. Cells* **93**, 51-54, 2009.
18. Salinas, O.H., et al. *Sol. Energy Mater. Sol. Cells* **90**, 2421-2428, 2006.
19. Bhat, S.V., et al. *Sol. Energy Mater. Sol. Cells* **95**, 2318-2321, 2011.
20. Koizhaiganova, R.B., et al. *Synth. Met.* **159**, 2437-2442, 2009.
21. Karim, M.R., et al. *J. Polym. Sci. A Polym. Chem.* **44**, 5283-5290, 2006.
22. Abdullah, O.G., et al. *J. Mater. Sci. Mater. Electron.* **26**, 5303-5309, 2015.
23. Mbhele, Z.H., et al. *Chem. Mater.* **15**, 5019-5024, 2003.
24. Gogoi, P., et al. *Prog. Org. Coat.* **77**, 87-93, 2014.
25. Gogoi, P., et al. *J. Appl. Polym. Sci.* **132**, 41490(1-9), 2015.
26. Patra, N., et al. *Compos. Part B Eng.* **43**, 3114-3119, 2012.
27. Mo, Z., et al. *J. Appl. Polym. Sci.* **112**, 573-578, 2009.
28. Sharma, S., et al. IEEE J. Photovolt. **5** (6), 1665-1673, 2015.